



Universiteit
Leiden
The Netherlands

Delivery of siHIF-1 α to reconstruct tumor normoxic microenvironment for effective chemotherapeutic and photodynamic anticancer treatments

Chen, X.; Jin, R.; Jiang, Q.; Bi, Q.; He, T.; Song, X.; ... ; Nie, Y.

Citation

Chen, X., Jin, R., Jiang, Q., Bi, Q., He, T., Song, X., ... Nie, Y. (2021). Delivery of siHIF-1 α to reconstruct tumor normoxic microenvironment for effective chemotherapeutic and photodynamic anticancer treatments. *Small*, 17(25). doi:10.1002/sml.202100609

Version: Publisher's Version

License: [Licensed under Article 25fa Copyright Act/Law \(Amendment Taverne\)](#)

Downloaded from: <https://hdl.handle.net/1887/3242878>

Note: To cite this publication please use the final published version (if applicable).

Delivery of siHIF-1 α to Reconstruct Tumor Normoxic Microenvironment for Effective Chemotherapeutic and Photodynamic Anticancer Treatments

Xiaobing Chen, Rongrong Jin, Qian Jiang, Qunjie Bi, Ting He, Xu Song, Matthias Barz, Hua Ai, Xintao Shuai,* and Yu Nie*

The tumor hypoxic microenvironment not only induces genetic and epigenetic changes in tumor cells, immature vessels formation for oxygen demand, but also compromises the efficiency of therapeutic interventions. On the other hand, conventional therapeutic approaches which kill tumor cells or destroy tumor blood vessels to block nutrition and oxygen supply usually facilitate even harsher microenvironment. Thus, simultaneously relieving the strained response of tumor cells and blood vessels represents a promising strategy to reverse the adverse tumor hypoxic microenvironment. In the present study, an integrated amphiphilic system (RSCD) is designed based on Angiotensin II receptor blocker candesartan for siRNA delivery against the hypoxia-inducible factor-1 alpha (HIF-1 α), aiming at both vascular and cellular “relaxation” to reconstruct a tumor normoxic microenvironment. Both *in vitro* and *in vivo* studies have confirmed that the hypoxia-inducible HIF-1 α expression is down-regulated by 70% and vascular growth is inhibited by 60%. The “relaxation” therapy enables neovascularization with more complete and organized structures to obviously increase the oxygen level inside tumor, which results in a 50% growth inhibition. Moreover, reconstruction of tumor microenvironment enhances tumor-targeted drug delivery, and significantly improves the chemotherapeutic and photodynamic anticancer treatments.

1. Introduction

Cancer development is a complex process, in which multiple genes dynamically and continuously change over time. This process is drastically influenced by the unique tumor microenvironment. Rapid metabolism and proliferation of tumor cells cause excessive oxygen consumption and require more blood supply to meet their demand for oxygen and nutrients.^[1] When the speed of vascularization could not match the requirements in time, a large number of disorganized and leaky tumor-associated vasculature is formed.^[2,3] These situations generally lead to low oxygen tension (hypoxia) in solid tumors, as one of the hallmarks during tumor progression. Tumor cells in hypoxia areas undergo adaptive genetic changes to survive, which enhances the risk of metastatic invasion, apoptotic resistance, and multidrug resistance.^[4] The malignant tumor cells also resultantly produce excessive angiogenic factors (e.g., vascular

endothelial growth factor (VEGF), transforming growth factors, fibroblast growth factor, angiopoietins, platelet-derived growth factor), which aggravate the formation of abnormally structured vessel. The disordered neovascularization hardly provides enough oxygen, leading to a more vicious circle among hypoxia, angiogenesis, and malignant tumor cells.^[3,5]


Anti-neovascularization therapy is one of most widely used strategies to block the so-called malignant loop.^[6,7] However, antiangiogenic drugs directly targeting VEGF to reduce tumor blood supply seems to be oversimplified and rough, which did not improve clinical outcome.^[8] It is likely that the strategy creates an even more abnormal microenvironment characterized by enhanced hypoxia and acidosis.^[9] Alternatively, appropriately adjusting the blood supply could relieve the physiological stringent state of blood vessels. Therefore, vascular normalization and tumor neovascular regulation give some ingenious ideas for alleviating hypoxia, emerging as a reciprocal therapeutic paradigm. This knowledge sets the ground for novel “relaxation” therapies.^[10–15] As a sensor for intratumoral hypoxia and high pressure, angiotensin II (Ang II) might be a promising target. The Ang-II receptor blockers, could appropriately decrease

X. Chen, Dr. R. Jin, Dr. Q. Jiang, Q. Bi, T. He, Dr. X. Song,
Prof. H. Ai, Prof. Y. Nie
National Engineering Research Center for Biomaterials
Sichuan University
Chengdu 610064, P. R. China
E-mail: nie_yu@scu.edu.cn

Prof. M. Barz
Leiden Academic Center for Drug Research (LACDR)
Leiden University
Einsteinweg 55, Leiden 2333 CC, The Netherlands

Prof. M. Barz
Institute of Organic Chemistry
Johannes Gutenberg-University
Mainz Duesbergweg 10–14, 55099 Mainz, Germany

Prof. X. Shuai
PCFM Lab of Ministry of Education
School of Chemistry and Chemical Engineering
Sun Yat-sen University
Guangzhou 510275, P. R. China
E-mail: shuaixt@mail.sysu.edu.cn

 The ORCID identification number(s) for the author(s) of this article can be found under <https://doi.org/10.1002/smll.202100609>.

DOI: 10.1002/smll.202100609

VEGF expression, reduce the abnormal vascular density, and increase vessel wall thickness.^[16–18] Thus, it could reduce vasculature leakage, consequently enhanced tumor tissue perfusion, and relieve hypoxia.^[19,20]

Another link of the vicious circle is the tumor cells itself. Killing tumor cells by cytotoxic drugs is the most direct and established therapeutic strategy, but often displays an unsatisfying outcome.^[21] Alternatively, adjusting the tumor cell response to the microenvironment has been found to be a promising strategy that might interrupt the loop. The key factor of tumor cells responding to hypoxia stress is the overexpressed hypoxia-inducible factor-1 alpha (HIF-1 α) in most carcinoma cells.^[22] The responsive up-regulated HIF-1 α is able to activate the gene expressions for cancer development promotion, including angiogenesis, tumor cell malignant proliferation, glucose metabolism, and metastasis.^[23] And then, inhibition of HIF-1 α has been considered to be a judicious and efficient approach to relax the stress of tumor cells in the hostile microenvironment.^[1]

According to previous researches, the sustained hypoxic environment inside the tumor tissues seriously weakened the conventional therapeutic methods either directly or indirectly.^[24] In terms of chemotherapy, hypoxia induces cellular adaptations to compromise the effectiveness, such as upregulated P-glycoprotein expression for drug resistance.^[25] The drug delivery efficiency was also dramatically impaired by the stringent and disordered blood vessels.^[26] Besides, photodynamic therapy (PDT) is an obvious oxygen-dependent treatment, which activates photosensitizer for energy transferring to the surrounding O₂ and produces reactive oxygen species (ROS) for tumor destruction. The lack of oxygen seriously hampers the PDT performance by restraining sufficient ROS generation from photosensitizer.^[27] Thus, regulation and reconstruction of the tumor normoxic micro-environment, especially for hypoxic alleviation is of great importance for PDT.

In view of current challenges, we hypothesize that combining the angiotensin inhibitor and HIF-1 α siRNA into one nanosystem could achieve a synergistic effect on reconstruction of tumor microenvironment. Besides, it was expected that the remodulated conditions could improve medicine accumulation and oxygen content for chemotherapeutic and photodynamic treatments. As a proof-of-concept demonstration, an integrated delivery system (RSCD) based on Ang-II receptor (AT₁R) blocker candesartan (CD) for HIF-1 α siRNA delivery has been designed, aiming at both vascular and tumor cellular interactive “relaxation” therapy for tumor microenvironment reconstruction (**Scheme 1**). CD was modified as the hydrophobic part, while the cationic dendritic arginine was selected as hydrophilic segment for gene condensation and high transfection efficiency.^[28,29] These two parts were linked with disulfide bond to make the product microenvironment responsive.^[30,31] After assembling with siRNA, RSCD gene complexes were further coated with a disulfide modified hyaluronic acid (HA-SS-COOH) to construct HA-RSCD/siRNA ternary complexes for targeted gene delivery. Finally, in vivo hepatic tumor model was employed for evaluation of the relaxation alone and combination therapies.

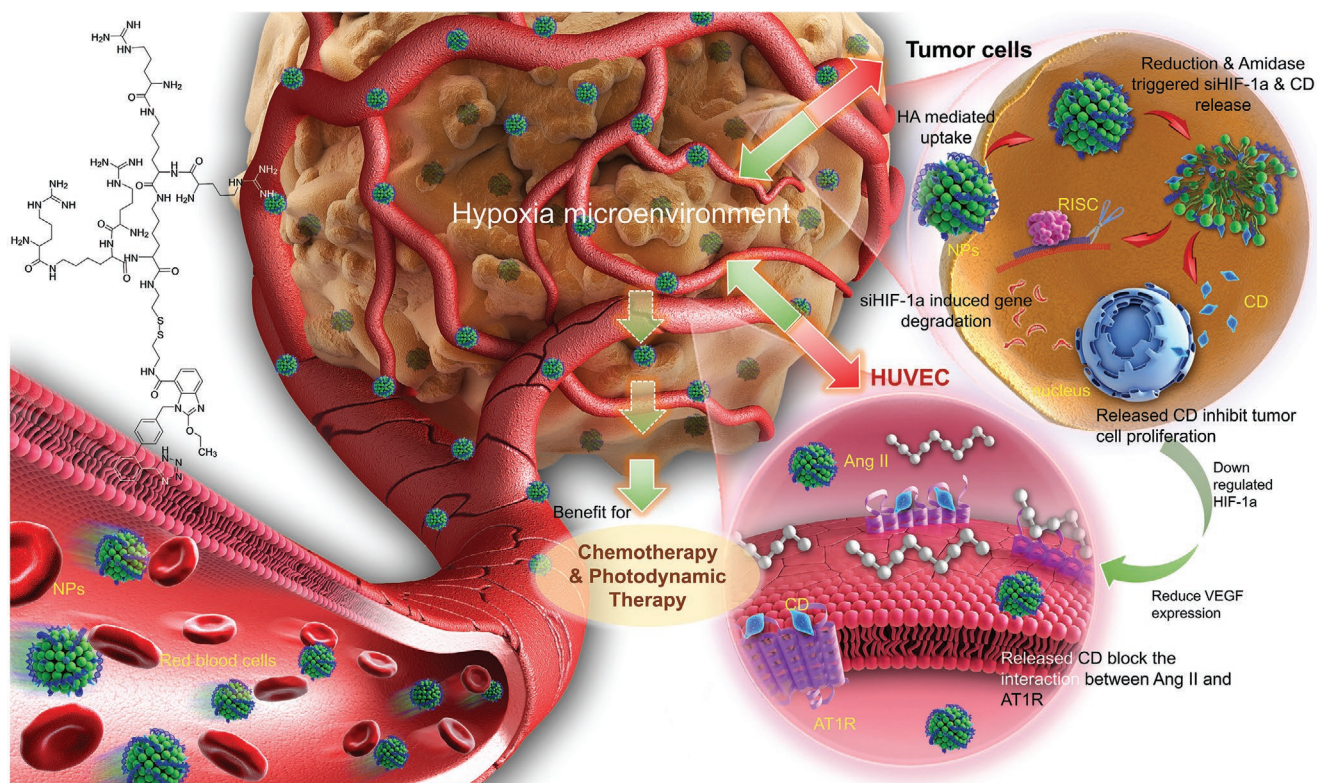
2. Results and Discussion

2.1. Synthesis and Characterization of RSCD

Amphiphilic lipopeptides can spontaneously self-assemble to form ordered nanostructures in water, and therefore conveniently mimic the architectures and functions of natural viruses for efficient nucleic acid delivery.^[32] Our workgroup has designed and synthesized a series of cationic amphiphilic lipopeptides (RLS) for structure-activity relationship studies, aiming at better supramolecular assembly, nuclear acid complexation, and gene transfection.^[28,33–35] Meanwhile, we found covalent link of drug/probe as main part of gene carrier may provide a straightforward technique to increase the drug loading efficiency and imaging accuracy with assisted and synergistic effects.^[29,33,36] Thus, as analog of RLS, RSCD molecule maintained the same cationic hydrophilic part to ensure the satisfactory gene delivery efficiency. And CD was linked with dendritic arginine through a disulfide bond as the hydrophobic segment of the amphiphile. The synthesis of RSCD is shown in **Figure 1**. The obtained compounds were confirmed using ¹H-NMR and MALDI-TOF MS (Figure S1, Supporting Information). In the ¹H-NMR spectrum of RSCD, characteristic peaks of CD at δ 1.21 ppm (t, -CH₃), 4.53 ppm (s, -OCH₂-) and 6.67–7.69 ppm (m, Ar-H), cystamine's peaks at δ 2.51–3.03 ppm (m, -CH₂CH₂-) and characteristic peak of arginine dendritic molecule (compound 2) at δ 2.95, 3.14 ppm (-NHCH₂-) all appeared. MS (MALDI-TOF-MS): calcd.1015.60 (M+H⁺). Drug loading efficiency is calculated to be 43%, according to the molecular weight of RSCD. After assembling with RLS,^[28] the size of RSCD vesicles was \approx 110 nm, and the zeta potential was +25.7 mV (**Figure 2A**).

2.2. Formation and Characterization of RSCD/siRNA and HA-RSCD/siRNA Complexes

The RSCD assemblies were dropwise added to siRNA solution followed by gently mixing for gene complexes (RSCD/siRNA) formation. The gene complexes were characterized by size distribution and zeta potential measurement (**Figure 2A**). It was clear that with the increased N/P ratios from 5 to 30, the Z-average size of the complexes displayed a descending trend (from 200 to 140 nm), while zeta-potential increased from 6 to 31 mV. Negatively charged HA-SS-COOH was gradually added into the pre-prepared RSCD/siRNA (N/P 20) complexes for ternary HA-RSCD/siRNA complexes fabrication, showing decreased zeta potential of -10.8 mV (coating to siRNA = 10, w/w) (**Figure 2B**). Morphology of the RSCD assemblies and HA-RSCD/siRNA complexes were observed by transmission electron microscope (TEM, **Figure 2C,D**), showing spherical particles with an average diameter of around 120 and 250 nm, respectively. Cationic RSCD assemblies showed complete siRNA condensation at N/P ratio of 5 without siRNA migration in agarose gel (**Figure S2**, Supporting Information). And addition of negatively charged HA-SS-COOH (with coating/siRNA weight ratios of 1–50) did not significantly affect the association between siRNA and RSCD as siRNA remained in the loading well (**Figure S2**, Supporting Information).



Scheme 1. Candesartan conjugate-based assemblies for siHIF-1 α delivery to reconstruct tumor normoxic microenvironment for effective chemotherapeutic and photodynamic anticancer treatments. The integrated amphiphilic delivery system (RSCD) composed of Ang-II receptor blocker candesartan (CD) and arginine-rich periphery was fabricated for siHIF-1 α delivery, aiming at both vascular and tumor cellular “relaxation” and consequently reversed the tumor hypoxia situation. The relaxed microenvironment is proposed to promote the following chemo/photodynamic therapy efficiency. The nano-system was internalized by HA-receptor mediated endocytosis, followed with the siHIF-1 α and candesartan (CD) release after de-shielding process and the configuration damage. The released siRNA knocked down HIF-1 α overexpression induced by the stress reaction of tumor cells to hypoxia, leading to the suppression of undisciplined tumor growth. Moreover, its downstream VEGF secretion also exhibits a cascading reduction, resulted in a scarce HUVECs anagenesis. CD as the hydrophobic segment of carries reverted back to the pharmacologically active moiety, and parallelly targeted to tumor cell proliferation and normalized neovascularization by blocking the interaction between AngII and AT1R. The reconstruction of tumor normoxic microenvironment could enhance tumor-targeted drug delivery, and significantly improve the chemotherapeutic and photodynamic anticancer treatment.

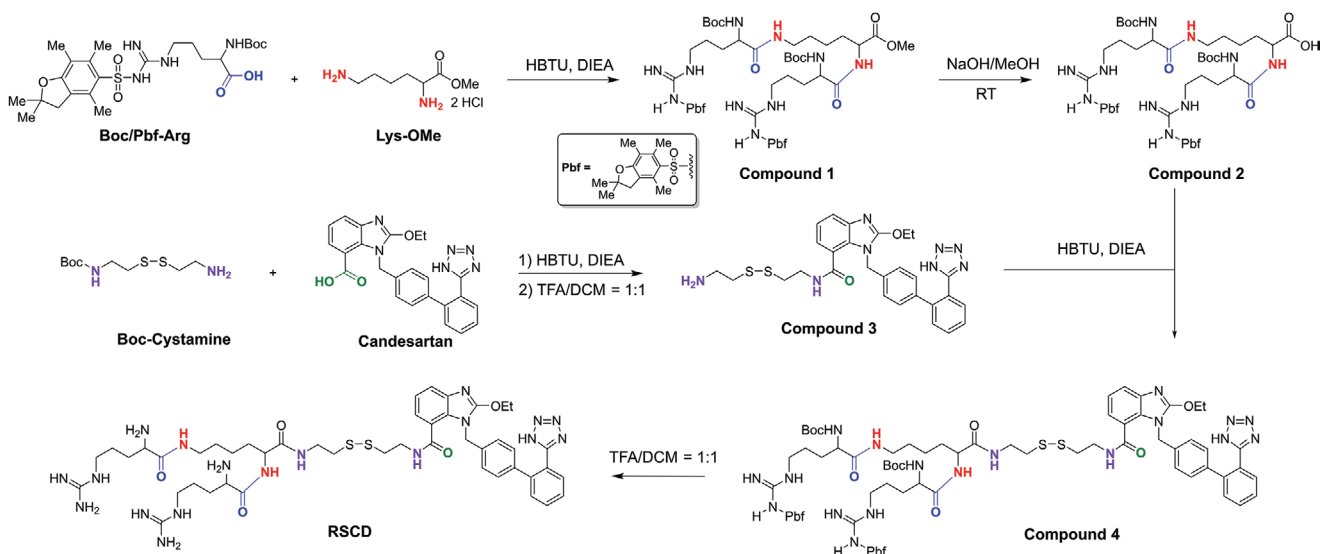


Figure 1. The chemical synthetic route of candesartan conjugation-based siRNA delivery system (RSCD).

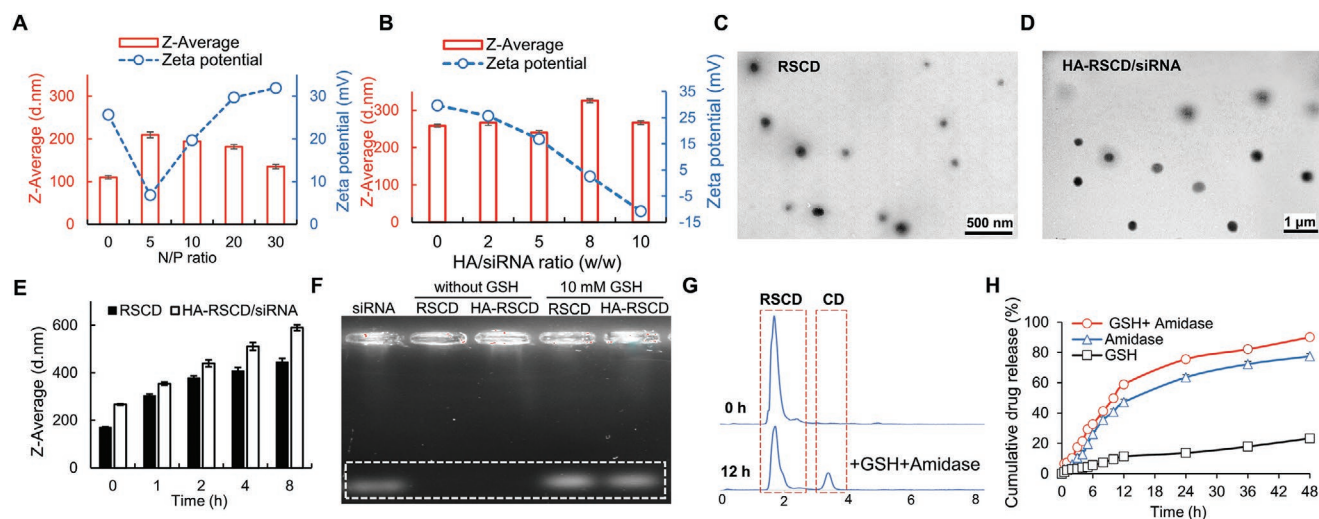


Figure 2. Physicochemical characterization gene complexes (RSCD/siRNA binary and HA-RSCD/siRNA ternary complexes) in the preparation and reductive conditions. A) Size and zeta potential of RSCD/siRNA binary complexes at different N/P ratios. B) Size and zeta potential of HA-RSCD/siRNA ternary complexes (N/P 20) with different HA/siRNA ratios. C) Morphology observation of optimized RSCD assemblies and D) HA-RSCD/siRNA complexes (N/P 20, HA/siRNA 10, w/w) by transmission electron microscope (bar = 500 nm and 1 μ m, respectively). E) Size variation of RSCD and HA-RSCD gene complexes in the presence of 10 mM GSH for 8 h incubation. F) Release behavior of siRNA from the gene complexes (RSCD and HA-RSCD) with or without glutathione (GSH, 10 mM) after 2 h-incubation. G) High performance liquid chromatogram (HPLC) of RSCD before and after incubation with GSH (10 mM) and amidase (10 μ M) for 12 h. H) Quantitative release profiles of candesartan from RSCD assemblies by HPLC.

Next, the status of gene complexes in reductive and amidase abundant solution for tumor microenvironment mimicking was investigated. The particle sizes of RSCD and HA-RSCD/siRNA were dramatically increased and became up to threefold larger at 8 h (Figure 2E), after incubation in 10 mM glutathione (GSH) solution. Such disintegration efficiently led to the siRNA liberation, verified by the visible new bands from both RSCD and HA-RSCD complexes in the gel retardation assay (Figure 2F). Besides, the release profile of CD from the RSCD assemblies was investigated by reverse-phase high performance liquid chromatography (HPLC) under reductive and amidase-rich conditions. (Figure 2G,H). In the conditions of GSH alone, the release of CD was obviously slow, and the cumulative release rate could only reach 23% for 48 h (Figure 2H). By contrast, the release was dramatically accelerated with amidase, indicating the hypersensitive response of amide bond.^[37,38] In particular, when RSCD assemblies were exposed to the intracellular level of 10 mM GSH and amidase simultaneously, the release was markedly facilitated, reaching \approx 60% within 12 h and 90% after 48 h incubation.

2.3. Cellular Uptake and Intracellular Trafficking of RSCD and HA-RSCD Complexes

The interaction between gene complexes and cells was assessed by confocal laser scanning microscopy (CLSM), using Cy5-labeled siNC (Figure 3A–D). HepG2 cells treated with HA-RSCD complexes displayed much stronger red fluorescence than those with RSCD complexes incubation, especially at the very beginning (0.5 h). (Figure 3A) The mean fluorescence intensity was accordingly higher, (Figure 3B) which was probably attributed to HA receptor-mediated recognition.^[39,40] Following, the late endosomes/lysosomes were labeled with LysoTracker (green) for intracellular trafficking (Figure 3C). It

was clear that many red fluorescent spots were located at the cell membranes in both HA-RSCD and RSCD groups at 2 h, while yellow fluorescent spots arose from the colocalization of siNC (red) with endo/lysosomes (green) appeared after 4 h incubation. According to more accurate evaluation by Pearson's correlation (R_r) (Figure 3D), a stronger decrease of R_r value was observed in the HA-RSCD group than that of RSCD at 6 h, showing more efficient and faster endosome escape.^[40]

2.4. Silence of HIF-1 α and Downregulation of its Downstream VEGF Expression

Hypoxic stress induced HIF-1 α overexpression activates transcription of several downstream targeted genes for tumor microenvironment adaption.^[41] Efficient silence of HIF-1 α and its related downstream genes could react back to the environment, depending on the successful gene transport into tumor cells. Data of q-PCR indicated that the HIF-1 α mRNA levels were significantly lower in HepG2 cells transfected with the HA-RSCD/siHIF-1 α (with 75% decrease) and RSCD/siHIF-1 α complexes (with 58% reduction) than the positive controls (Lipo/siHIF-1 α , 44% reduction) (Figure 3E). The improved silence efficiency was attributed to efficient gene delivery capacity of RSCD as well as satisfactory cellular internalization by HA coating.^[42] Meanwhile, it could find that free CD had no evident effect on HIF-1 α downregulation, which was also confirmed by the similar down-regulation efficiency (\approx 40%) in the RLS/siHIF-1 α and RLS/siHIF-1 α +CD treated group.

One of the most important downstream genes after HIF-1 α translocation is VEGF, which drives tumor angiogenesis for oxygen supply.^[4,43] Thus, the influence on VEGF was also detected by q-PCR (Figure 3F). After HA-RSCD/siHIF-1 α treatment, the mRNA of VEGF was reduced by around 70%,

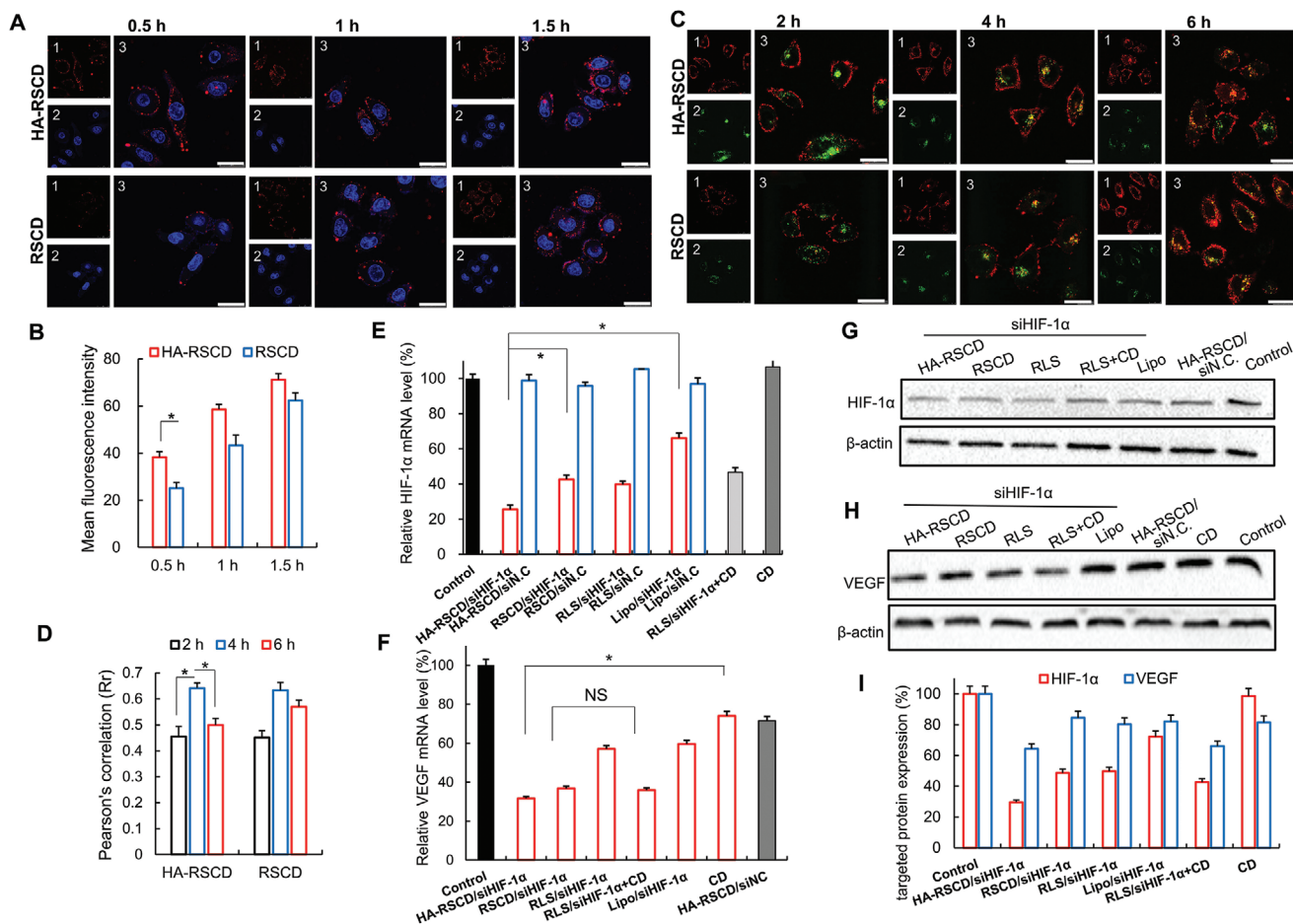


Figure 3. Intracellular fate and HIF-1 α related gene silencing effect of various siRNA complexes in HepG2 cells. A) Observation of cellular internalization at indicated time points by confocal laser scanning microscopy (CLSM). Channel 1: red fluorescence for Cy5-labeled siRNA, Channel 2: blue fluorescence for Hoechst 33342 stained nucleus, Channel 3: overlay of 1 and 2. B) Semi-quantitative analysis of the cellular uptake of various gene complexes by red fluorescence intensity at different times. C) Assessment of endosomal escape. Channel 1: Cy5-labeled siRNA (red), Channel 2: LysoTracker stained endosomes (green), Channel 3: overlay of 1 and 2. (Scale bars: 25 μ m). D) The endosomal release efficiency evaluation by Pearson's correlation (Rr) calculation from CLSM images. Rr is considered to represent the colocalization degree of Cy5 and LysoTracker Green. qRT-PCR analysis of E) HIF-1 α and F) VEGF suppression on mRNA levels in HepG2 cells after treatment with various formulations. G) Western blot analysis of HIF-1 α suppression and H) down-regulation of VEGF at protein levels in HepG2 cells after transfection by various formulations. I) Semi-analysis of the light intensities of HIF-1 α and VEGF protein expression as the ratio of target protein to β -actin from western blot results. The data are shown as the mean \pm s.d. ($n = 5$). *, $p < 0.05$ and NS, no significance.

compared with 25% and 40% decrease for free CD incubation and lipofectamine transfection, respectively. More importantly, the levels of VEGF mRNA in the RSCD/siHIF-1 α and RLS/siHIF-1 α +CD treatment groups were decreased by \approx 60%, compared with 40% reduction for RLS/siHIF-1 α . This difference has confirmed the co-effect of CD and siHIF-1 α on the down regulation of VEGF, either in the integrated RSCD/siHIF-1 α group or the mixed RLS/siHIF-1 α +CD group. Following, similar trends of HIF-1 α (Figure 3G,I) and VEGF (Figure 3H,I) protein down-regulation in varied groups were analyzed by western blot (WB).

2.5. The Interactive Effects on Anti-Tumor Cell Proliferation and Anti-Angiogenesis between HepG2 Cells and Human Umbilical Vein Endothelial Cells

Both tumor cells and endothelial cells in the hypoxic tumor micro-environment could develop a hypoxic cellular response.

Thus, the parallel and cascade effects of siHIF-1 α and CD on anti-proliferation, anti-angiogenesis, and migration inhibition between HepG2 cells and human umbilical vein endothelial cells (HUVEC) were explored as schematic diagrams in Figure 4A.

HIF-1 α gene upregulation was the most typical character for tumor cells suffered from hypoxia, which promotes cell proliferation in harsh conditions.^[1] Thus, both HepG2 cells and HUVECs were directly incubated with various siHIF-1 α complexes under hypoxic-mimicking condition. It was clear that HA-RSCD formulation without therapeutic gene display negligible cytotoxicity toward both of them (Figure 4B). While gene formulations with siHIF-1 α , especially the HA-RSCD/siHIF-1 α , showed dramatic tumor killing activity. It was obviously stronger than the parallel effect on HUVEC, suggesting the dominating role of HIF-1 α in tumor cell proliferation. (Figure 4B) In addition, free CD also suppressed the tumor cell proliferation with \approx 20% inhibition rate, which was in accordance with others'

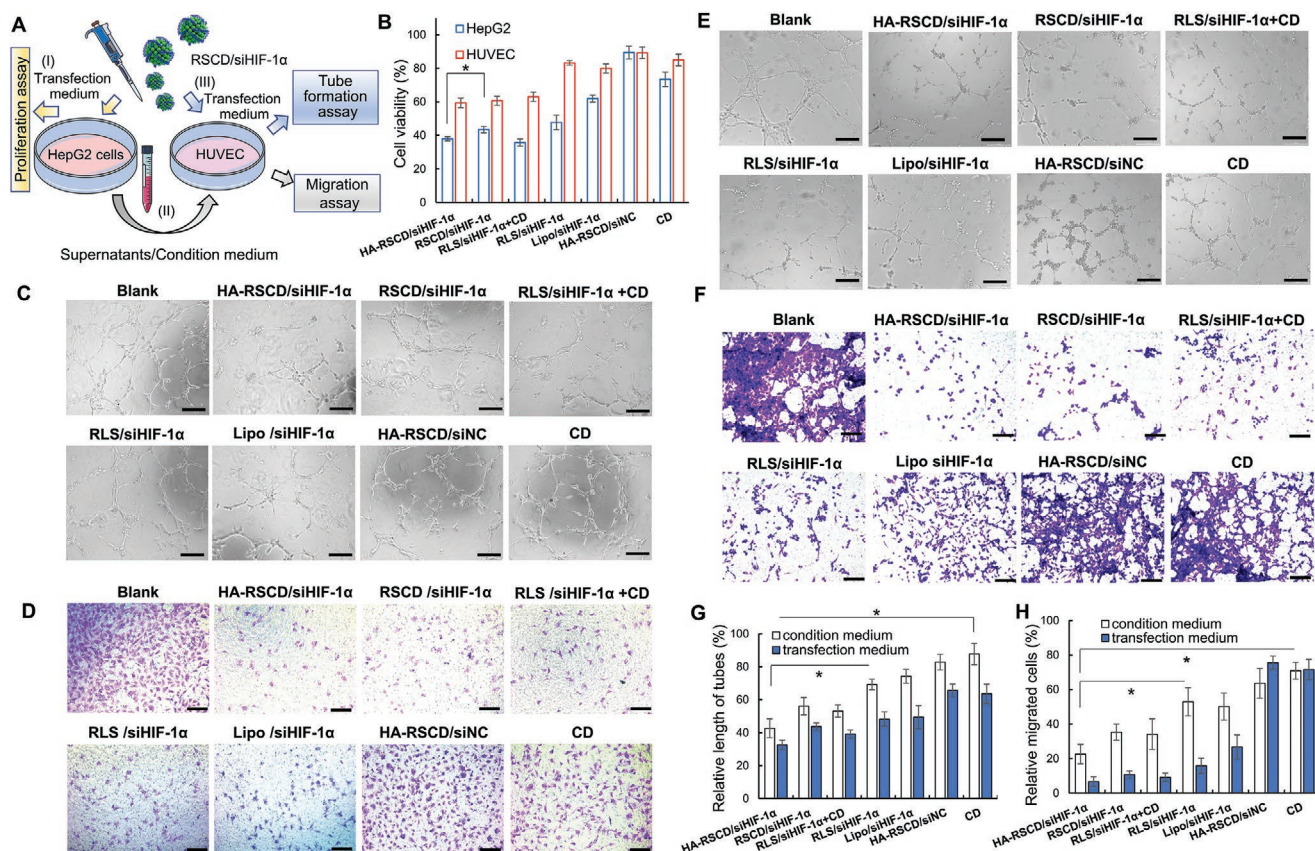


Figure 4. The parallel and cascade effects on anti-tumor cell proliferation and anti-angiogenesis between HepG2 cells and human umbilical vein endothelial cells (HUVEC). A) The schematic diagram of mimic in vitro co-culture system of tumor and vascular cells treated with various therapeutic formulations. I) Add therapeutic formulations (transfection medium) to HepG2 tumor cells for cellular proliferation measurement. II) Supernatants (condition medium) from the above step are collected after 48 h incubation and added into HUVEC, followed by the tube formation and migration assay. III) Add therapeutic formulations (transfection medium) directly into the HUVEC, followed by tube formation and migration assay as well as cell growth assay. B) The parallel effect on cell viability of HepG2 cells and HUVEC after treatments with various therapeutic formulations for 24 h. The dosage of siHIF-1 α was 2 $\mu\text{g mL}^{-1}$. C) The cascade tubule formation status of HUVEC cells after 4 h-incubation with different condition medium. D) Representative microscopic images of cascade HUVEC migration in Boyden chamber after incubation with different condition medium for 24 h. HUVEC cells were seeded on the top chamber, and condition medium was added into the bottom chamber. E) The tubule formation of HUVEC cells on Matrigel after incubation with various transfection mediums. F) Representative microscopic images of HUVEC in Boyden chamber migration assay after treatment with transfection medium. Scale bars = 200 μm . G) Semi-quantitative results of the tubule formation by relative tube length to the blank group calculated from Image J software. H) Semi-quantitative evaluation of HUVEC migration in Boyden chamber after incubation with condition medium from HepG2, or transfection with different formulations. The data are shown as the mean \pm s.d. ($n = 5$). * $p < 0.05$.

studies.^[16,17] And groups with both siHIF-1 α and CD (including HA-RSCD/siHIF-1 α , RSCD/siHIF-1 α and RLS/siHIF-1 α +CD) exhibited better anti-proliferation than the individual ones (such as RLS/siHIF-1 α , Lipo/siHIF-1 α and CD), indicating favorable synergetic effect on proliferation suppression.

Another main outcome of HIF signaling is angiogenesis, which attempts a compensation of the oxygen deficiency in the tumor tissue. Endothelial cells would respond to extra VEGF secreted from tumor cells in hypoxia to realize neovascularization.^[44] In order to mimic the process, HUVECs were incubated with condition medium of tumor cells. First, HepG2 cells transfected with gene complexes were cultured in the hypoxic condition for 48 h. And then, the culture supernatants were added to HUVECs for tube formation examination. In the blank group, cells end-to-end aligned themselves and formed microvascular networks with cord-like structures, which was a facilitation sign of angiogenesis (Figure 4C). In contrast, HUVECs in

groups with siHIF-1 α (HA-RSCD/siHIF-1 α , RSCD/siHIF-1 α , RSCD/siHIF-1 α +CD, RLS/siHIF-1 α and Lipo/siHIF-1 α) or CD (HA-RSCD/siNC and CD) could only form incomplete and short tubes to different extent.

Cell migration ability of HUVECs is critical for the tube formation.^[45] Migrating endothelial cells must break their basement membrane and transverse through it to form new vessels. So, we investigated whether the siHIF-1 α delivery could restrain HUVECs migration in the chemotaxis of tumor cell supernatant. Compared to blank group as well as monotherapy treatment groups (RLS/siHIF-1 α , Lipo/siHIF-1 α , HA-RSCD/siNC or CD), the combination groups (including HA-RSCD/siHIF-1 α , RSCD/siHIF-1 α , and RLS/siHIF-1 α +CD) showed obvious attenuation in migration with less cells invaded to the under surface of the top well membrane (Figure 4D).

Apart from the paracrine influence of tumor cells, direct down-regulating HIF-1 α and blocking the Ang II receptor by

CD in endothelial cells could also impair vascularization.^[3,23] It was found that HUVEC cells transfected with different formulations exhibited seldom tube formation with higher inhibitory effect than those incubated with condition medium. (Figure 4E) In terms of migration ability, the mobility of HUVECs that directly incubated with different formulations was also attenuated as expected. (Figure 4F). Besides, it seems that CD plays a more importantly suppressive role in tube formation of HUVEC than that in migration ability.

According to the average tube length (TL) calculation (Figure 4G), HA-RSCD/siHIF-1 α group exerted the lowest relative length of tubes ($\approx 42\%$) and the highest inhibition rate of around 60% (Figure S3A, Supporting Information) in the conditioned medium. This was attributed to the co-effect from CD and siHIF-1 α on HepG2 cells. Treatment of HA-RSCD/siNC complexes or free CD showed similarly weak inhibitory effects on tube formation ($\approx 12\%$). While the inhibition rate was $\approx 30\%$ for RLS/siHIF-1 α group, 44% for RLS/siHIF-1 α +CD and 46% for RSCD/siHIF-1 α group (Figure S3A, Supporting Information). These observations were in accordance with the VEGF expression of HepG2 cells incubated with different formulations. In line with tube formation results, HA-RSCD/siHIF-1 α group displayed the minimum number of migrated cells ($\approx 23\%$) and the highest inhibition rate around 77% (Figure 4H and Figure S3B, Supporting Information). Similar trends were found in transfection medium cultivation. (Figure 4G,H and Figure S3A,B, Supporting Information)

Overall, the HA-RSCD/siHIF-1 α formulation parallely relieved the stress response of tumor cells and HUVECs to the microenvironment, with direct inhibition of cellular proliferation, cascading reduction of abnormal vessel formation, and blocking endothelial cell mitigation.

2.6. “Relaxation” Therapeutic Effect of HA-RSCD/siHIF-1 α Complexes on Reconstruction of Tumor Microenvironment In Vivo (Tumor Inhibition, Blood Vessel Situation, and Hypoxia Degree etc.)

Next, we examined the effects of HA-RSCD/siHIF-1 α complexes on reconstruction of tumor microenvironment, including the tumor growth inhibition, blood vessel situation, and hypoxia degree in the HepG2 xenograft tumor model in vivo. The size of tumors treated with saline increased rapidly over the course of therapy and reached a final tumor volume of ≈ 4.5 -fold larger than the original one, while the significant tumor growth inhibition was observed in HA-RSCD/siHIF-1 α treated group with only 2.3 -fold increase in the final tumor volume. (Figure 5A) An approximately threefold volume increase was observed in RSCD/siHIF-1 α treated mice, which was similar to the mixture (RLS/siHIF-1 α +CD) group. The difference might result from the enhanced accumulation effect of hyaluronic acid. There was no significant toxicity, showing no obvious body weight loss in HepG2-bearing mice during the treatment (Figures S4 and S5, Supporting Information). The hematoxylin-eosin (H&E) staining of tumor sections showed that HA-RSCD/siHIF-1 α induced the most obvious apoptosis and necrosis in tumor tissues (Figure 5B).

Inspired by these encouraging results, we aimed to verify the role of HIF-1 α silencing in the tumor growth suppression. First, we analyzed the extent of hypoxia in tumors by pimonidazole (Hypoxyprobe), to determine whether HA-RSCD/siHIF-1 α treatment interfered with oxygenation of tumor tissues. From the images, the strongest green fluorescence of hypoxia signals was observed in saline group, while those in HA-RSCD/siHIF-1 α and RSCD/siHIF-1 α treatments were significantly lower (Figure 5C). Compared to the saline, the hypoxyprobe signal intensity in HA-RSCD/siHIF-1 α group decreased by $\approx 70\%$, indicating hypoxia alleviation and vessel function improvement (Figure S6, Supporting Information).

Followingly, the protein expression patters of HIF-1 α in the tumor tissues were assessed by immunofluorescence staining. Strong red fluorescence was observed in saline group, indicating large amount of HIF-1 α in the HepG2 cell xenograft tumor (Figure 5D). After RSCD/siHIF-1 α and the mixture (RLS/siHIF-1 α +CD) treatments, the HIF-1 α expression was reduced. Satisfyingly, the HA-RSCD/siHIF-1 α treatment could significantly decrease HIF-1 α protein expression to 15%, compared with 50% and 30% in saline and RSCD/siHIF-1 α treated group, respectively (Figure S7A,B, Supporting Information). The advantages of HA-RSCD/siHIF-1 α over RSCD/siHIF-1 α may be attributed to the increased recognition and fast cellular endocytosis by HA coating as verified above (Figure 3A).^[46]

Considering the synergistically inhibitory effect of siHIF-1 α and CD on endothelial cell migration and tube formation, we evaluated the status of in situ tumor vasculatures after receiving the above-described treatments. The paraffin tumor sections extracted from mice were double-stained with pericyte marker α -smooth muscle actin (α -SMA) and vessel marker CD31. Compared with other groups, the immunostaining of CD31 with HA-RSCD/siHIF-1 α treatment displayed a notable reduction in the number of blood vessels (Figure 5E). Besides, the vessels showed more normalization hallmarks in line with a relaxed or less stressed status, such as reduced vessel branching and relatively organized vessel morphology. While more chaotic and twisted vessel architectures were observed in the saline treated group.

Apart from endothelial cells, pericytes that surround blood vessels are also major components of blood vessels and the pericyte coverages along the vascular wall are the key signature of normalized tumor vessels. The higher degree of colocalization between CD31 and α -SMA implies more mature and normal vessels.^[2,13] It was clear that absent pericyte coverages and detached structures were observed in the saline group, whereas RSCD/siHIF-1 α and RLS/siHIF-1 α +CD groups showed a slight coverage increase. (Figure 5E) More importantly, after HA-RSCD/siHIF-1 α treatment, the green fluorescence profiles of CD31 largely overlapped with the red fluorescence of α -SMA (red) (Figure S8, Supporting Information) and the scatterplot of pixel intensities demonstrates a high degree of association between CD31 and α -SMA (Figure 5F) Previous studies have supported that as consequence of normalization, tumor vascular could alleviate hypoxia.^[47,48]

Overall, these results demonstrated that HA-RSCD/siHIF-1 α could postpone the tumor growth, induce normalization of tumor blood vessels and ameliorate tumor hypoxia, owing to the synergistic effect of siHIF-1 α and CD.

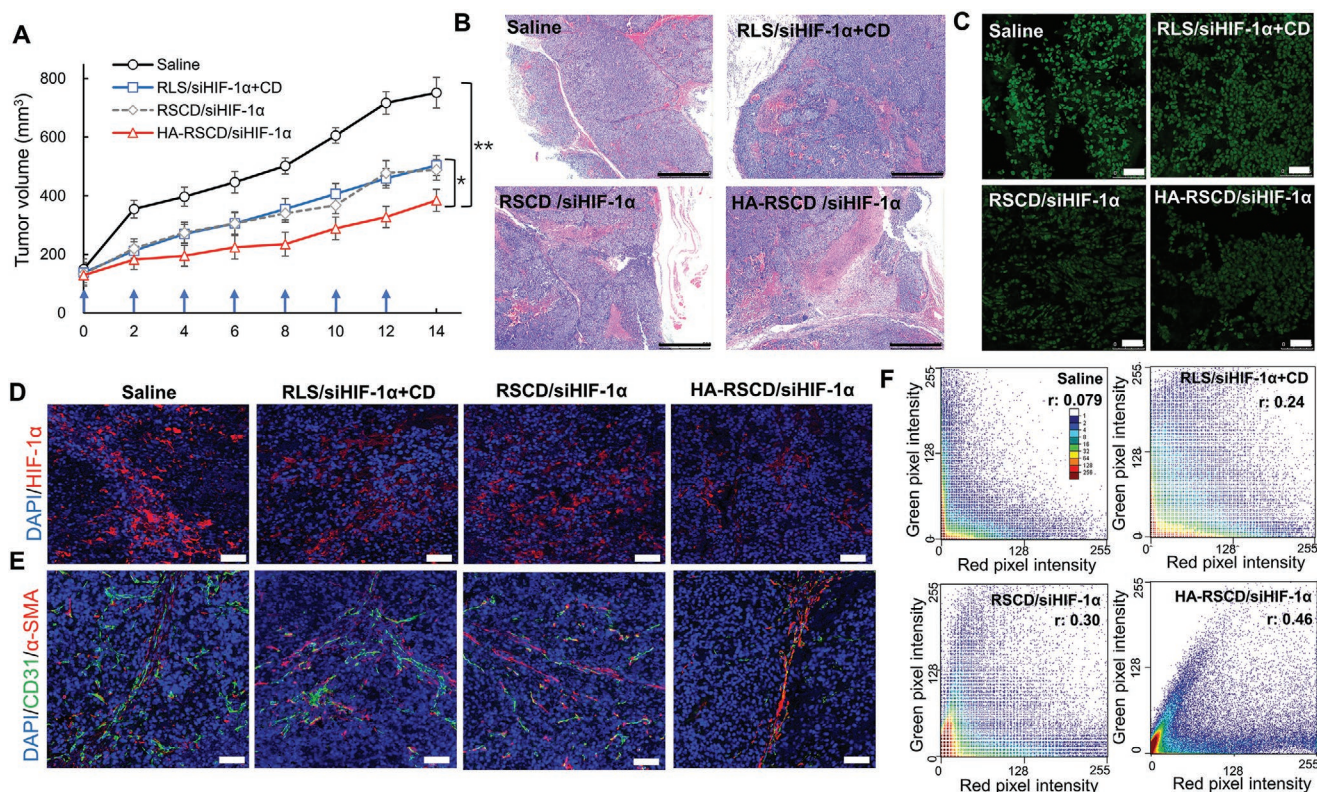


Figure 5. “Relaxation” therapeutic effect (tumor inhibition, blood vessel situation, hypoxia degree etc.) in BALB/c nude mice with HepG2 xenografts by HA-RSCD/siHIF-1 α complexes treatment. **A**) Tumor growth curve of mice after seven injections of the indicated formulations. * $p < 0.05$, ** $p < 0.01$. **B**) The hematoxylin-eosin (H&E) staining images of tumor tissue sections from HepG2-bearing mice after 14 days treatment with indicated gene complexes. Scale bars = 500 μm . **C**) Hypoxia evaluation by the immunofluorescence sections stained with hypoxyprobe-1-FITC-Mab1 (representative photographs). Scale bars = 20 μm . **D**) The immunofluorescence staining of HIF-1 α (red) in tumors treated by the indicated formulations. **E**) Determination of pericyte coverage on endothelium by co-staining of CD31 (green) and α -SMA (red) in tumor sections. Scale bars = 25 μm . **F**) Correlation graphs comparing the green and red channel in the images analyzed by “Scatter J” plugin of Image J software. “r” means Pearson’s coefficient.

2.7. Combination Therapy of HA-RSCD/siHIF-1 α and Doxorubicin

It has been recognized that normalization of tumor blood vessels can improve the perfusion and penetration of antitumor drugs.^[12,13,49] Thus, we evaluated the therapeutic effects of HA-RSCD/siHIF-1 α in combination with doxorubicin (at a dose of 5 mg kg⁻¹) in HepG2 xenografts (Figure 6A). Tumor size increased rapidly in the saline group as expected (Figure 6B), and the growth was moderately delayed after doxorubicin treatment alone by ≈ 310 mm³. What appears compelling was that pre-treatment with HA-RSCD/siHIF-1 α before doxorubicin obviously potentiated chemotherapy, which displayed a 60% reduction in tumor volume. Meanwhile, no body weight loss and obvious normal tissue damage were found during the doxorubicin administration nor the combination therapy (Figure 6C and Figure S9, Supporting Information). The H&E staining of tumor issue in the saline group displayed many chromatin and multinuclear tumorous cells (Figure 6D). While varying degrees of tumor necrosis and nucleus atypia were found in doxorubicin monotherapy and the synergetic treatment. Furthermore, TdT-mediated dUTP nick-end labeling (TUNEL) assay showed that combination therapy increased the number of TUNEL-positive tumor cells compared with

doxorubicin alone, indicating a more pronounced apoptosis induction in tumor tissue (Figure 6D and Figure S10, Supporting Information). In order to further demonstrate whether the enhanced therapeutic effect was ascribed to the enhanced doxorubicin penetration inside tumor tissue, the accumulation was then determined using IVIS Lumina Series III imaging system. Based on the ex vivo fluorescence intensity assay, it was found that the accumulation was really about twofold higher with HA-RSCD/siHIF-1 α pre-treatment than that of doxorubicin monotherapy group (Figure 6E–G). These results confirm that HA-RSCD/siHIF-1 α could reconstruct and normalize functional blood vessels and therefore enhance the accumulation of chemotherapeutics in tumors with the final effect of suppressing tumor growth.

2.8. Combination Therapy of HA-RSCD/siHIF-1 α and Chlorin e6 (Ce6) Liposomes Induced PDT

Abnormal tumor vasculature could not supply enough oxygen, which hampers the therapeutic efficacy of oxygen-dependent PDT.^[25,49] Hence, reconstructing the tumor microenvironment from hypoxic to normoxic is a promising method to potentiate PDT efficacy. Moreover, the normalized vascularization

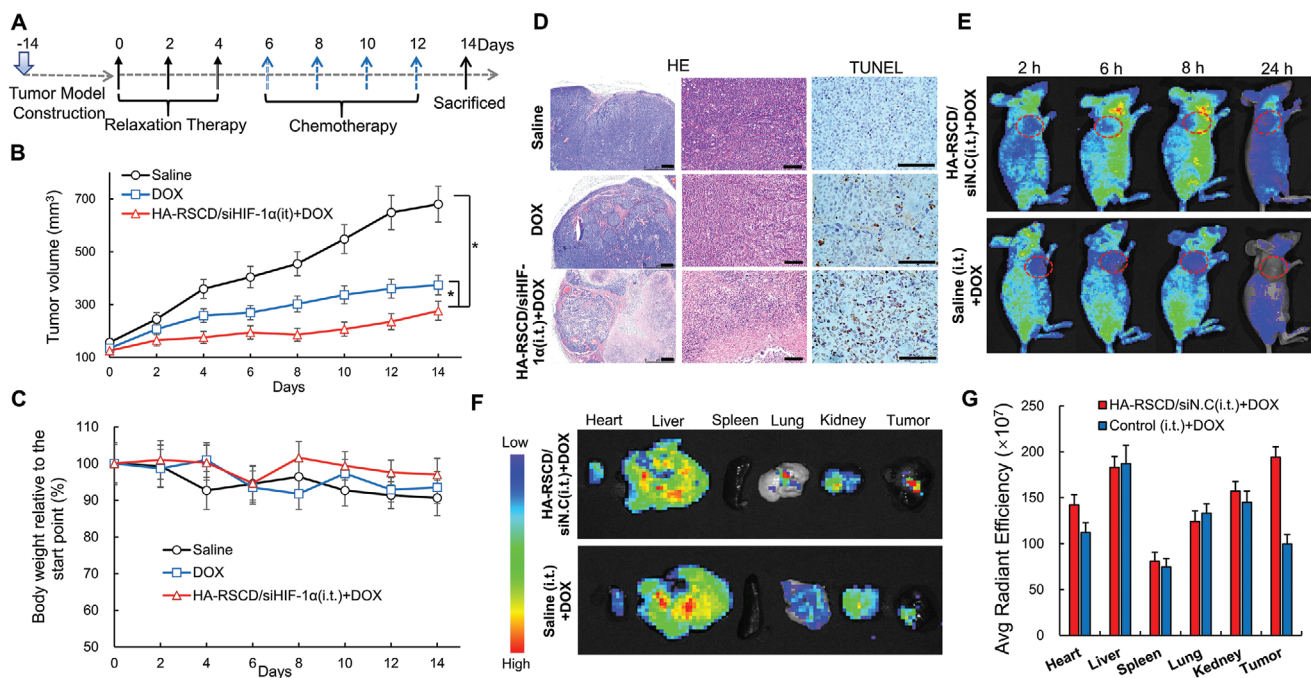


Figure 6. Combined therapeutic effect of “relaxation” treatment and chemotherapy (doxorubicin, DOX) on HepG2 subcutaneous xenografts. A) Administration schedule of combination relaxation/chemotherapy. The HepG2 tumor-bearing mice received HA/RSCD/siHIF-1 α by intratumor injection every 2 days for three injections and subsequently received additional doxorubicin intravenously every 2 days for four injections. B) Tumor growth curves during the treatment. (* $p < 0.05$). C) Body weight changes of mice during treatment. D) Histological studies with hematoxylin-eosin staining (H&E) and TdT-mediated dUTP nick-end labeling (TUNEL) staining of tumor sections after 14 days synergistic therapy. (Scale bars = 200 μ m) (NS, no significance). E) Fluorescence images of DOX trapping distribution in HepG2-bearing nude mice and F) organs (including tumors) excised from the mice at indicated time with or without “relaxation” pretreatment for three times with 2 days interval. G) Corresponding semiquantitative data of fluorescence signals of DOX from Figure 6F.

provides an opportunity for enhanced penetration of photosensor nanoparticles. As shown in **Figure 7A**, mice were injected with HA-RSCD/siHIF-1 α or saline on days 0, 2, and 4 and treated with Ce6 liposomes on day 6. Laser-irradiation was implemented in 24 h after Ce6 injection. The tumor growth (**Figure 7B**) and body weight (**Figure S11**, Supporting Information) were recorded for 14 days and a photograph of tumors collected from mice on last day (**Figure 7C**). As expected, mice after combination therapy showed the best tumor growth inhibition effect (63% inhibition ratio), which was dramatically better than the Ce6 liposomes mediated PDT alone (26% inhibition ratio). Both HE staining and immunohistochemical TUNEL staining of tumor sections suggested that the combination therapy promoted the apoptosis of tumor cells. (**Figure 7D**)

To understand the mechanism of the enhanced effect, tumor oxygenation and Ce6 liposomes accumulation in tumor site after three times treatments of HA-RSCD/siHIF-1 α were studied on day 6. Photoacoustic imaging (PA) was utilized to monitor the oxygenation status of tumor by measuring oxygenated and deoxygenated hemoglobin (Hb) at the wavelengths 850 and 750 nm, respectively. As collected by PA system (**Figure 7E,F**), the blood oxyhemoglobin level was increased after HA-RSCD/siHIF-1 α treatment. It was consistent with the above immunofluorescence staining results (**Figure 6**), which was beneficial from the normalization of tumor blood vessels. On the other hand, the captured fluorescent signals of Ce6 liposomes in the mice after HA-RSCD/siHIF-1 α treatments

showed much higher intensity at tumor site. (**Figure 7G**) While, the strongest signal came from the liver in the saline group, and signal at the tumor site was much dim. Ex vivo fluorescence images of representative tumors at 24 h post-injection of Ce6 liposome showed the same phenomena. (**Figure 7H,I**) It confirmed the normalized blood vessels could promote the Ce6 liposomes accumulation in tumor site.

3. Conclusion

The interplay of tumors and its microenvironments forms a vicious circle that aggravates the development of cancer. Precisely designed nano-systems simultaneously targeting tumor cells, blood vessels, and microenvironment not only provide promising opportunities to block the loop and remold the abnormal tumor conditions, but also benefit for combination with other therapeutic methods. In the present study, an integrity siRNA delivery system (RSCD) based on CD analog is conducted for synergistically inhibiting Ang II and HIF-1 α activation. The siRNA knocked down HIF-1 α expression by 70%, which relieved the tumorous sensitive response to hypoxia and consequently reduced VEGF secretion. Its cascading effect on angiogenesis was also demonstrated. After CD release by GSH/amidase treatment, it simultaneously lowered the stress of blood vessels and suppress tumor growth on hypoxia. The synergistic effect on remodeling tumor microenvironment

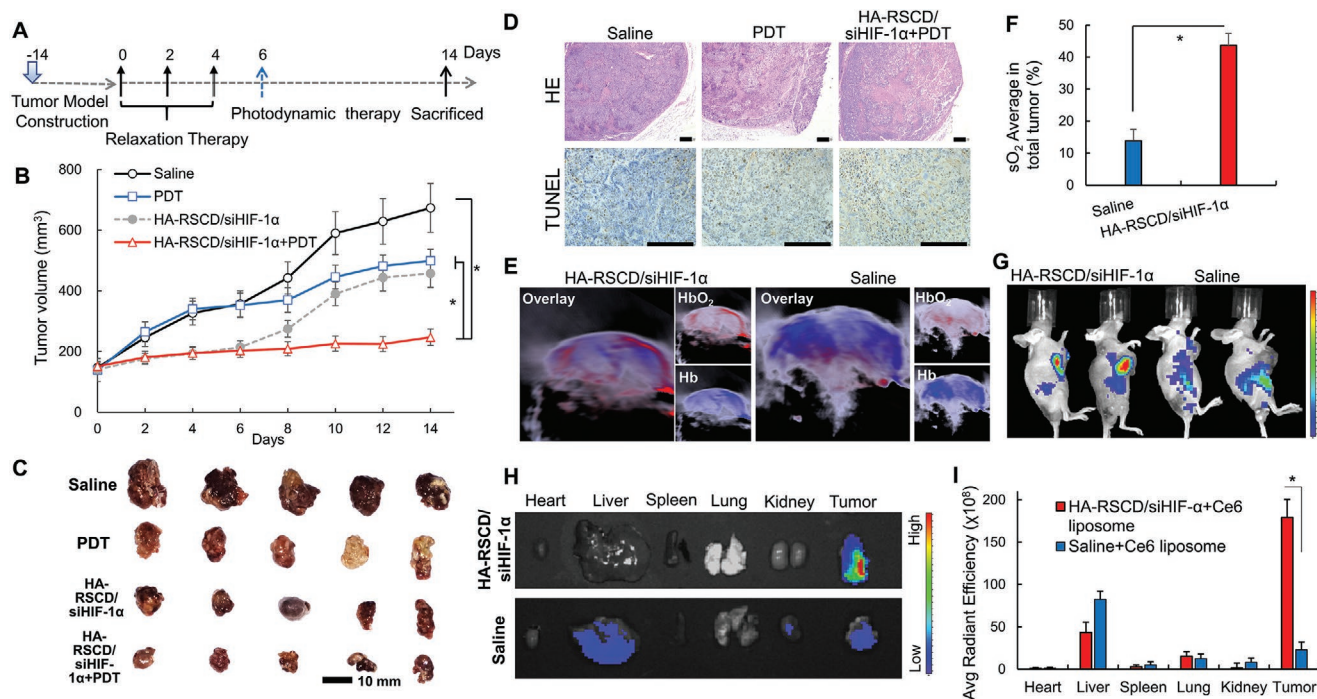


Figure 7. Combined therapeutic effect of “relaxation” treatment and photodynamic therapy (Ce6 liposomes) on HepG2 subcutaneous xenografts. A) Administration schedule of combination relaxation/photodynamic therapy. The HepG2 tumor-bearing mice first received HA/RSCD/siHIF-1 α by intratumor injection every 2 days for three injections. And then, additional Ce6 liposomes (5 mg kg⁻¹) were intravenously injected, with subsequent laser irradiation (660 nm, 100 mw cm⁻², 30 min) after 24 h following the last treatment. B) Tumor growth curves during the treatment. * $p < 0.05$. C) Photographs of tumors removed from the sacrificed mice after the last treatment. D) Histological studies with hematoxylin-eosin staining (H&E) and TdT-mediated dUTP nick-end labeling (TUNEL) staining of tumor sections after 14 days synergistic therapy. Scale bars = 200 μ m. E) Representative 2D photoacoustic (PA) images of HepG2 tumors on nude mice, measuring deoxygenated hemoglobin (Hb, $\lambda = 750$ nm) and oxygenated hemoglobin (HbO₂, $\lambda = 850$ nm) with or without the “relaxation” pretreatment. F) Quantification of the oxyhemoglobin saturation levels in tumors by PA imaging signal measurement. The oxygen saturation across the total tumor area (sO₂ Avr Total) was calculated using the ratio of the PA signals from oxygenated and total hemoglobin. G) Distribution of Ce6 liposomes in HepG2-bearing nude mice and H) excised organs (including tumors) after intravenous injection for 24 h, with or without “relaxation” pretreatment. I) Semi-quantitative results of fluorescent Ce6 signal in tumor and organs. (Excitation = 630 nm, emission = 700 nm).

attenuated the tumor development both in vitro and in vivo by inhibiting tumor cell proliferation and uncontrolled angiogenesis, which promotes a virtuous circle for tumor therapy. Meanwhile, the reconstructed normoxic microenvironment and normalized vessels could significantly improve the combination with chemotherapeutic and photodynamic anticancer treatment.

4. Experimental Section

Materials: RLS and HA-SS-COOH were prepared according to the previous technics.^[28,50] Boc/Pbf-Arg-OH and H-Lys-OMe-2HCl were from GL Biochem (P. R. China), N,N-diisopropylethylamine (DIEA), O-(benzotriazol-1-yl)-N,N,N',N'-tetramethyluronium hexafluorophosphate (HBTU) and trifluoroacetic acid were obtained from Astatech (China). CD was purchased from Meilunbio (China). Fetal bovine serum, lipofectamine 2000 reagent, and Dulbecco's modified Eagle's medium with high glucose were obtained from Life Technologies Corporation (USA). Endothelial cell medium (ECM) and HUVEC were from ScienCell (USA). The human Hepatocellular carcinoma (HepG2) cell line was obtained from Shanghai Institutes for Biological Sciences (China). LysoTracker Green DND-22 was from Life Technologies Corporation (USA). Antibodies against VEGF and human hypoxia-inducible factor-1 α (HIF-1 α) were purchased

from Abcam (USA). Antibodies against β -actin, goat anti-mouse IgG-HRP antibody, goat anti-rabbit IgG-HRP antibody, and crystal violet were obtained from Beyotime Biotechnology (China). Small interfering RNA targeting human HIF-1 α (siHIF-1 α) (sense strand, 5'-CGAUCAGCAGCUACACAdTdT-3' and antisense strand, 5'-UGUAGUAGCUGCAUGAUCGdTdT-3') and scrambled siRNA (N.C.) (sense strand, 5'-AGUUAACGACCAGUAGUCdTdT-3' and antisense strand, 5'-GACUACUGGUCGUUGAACdTdT-3') were provided by Shanghai GenePharma Co. Ltd. (China). Fluorescein-tagged scrambled siRNA (Cy5-siRNA) was synthesized by modifying 5'-end of the sense strand with fluorescein. Real-time PCR was performed by iScript cDNA synthesis kit and iQ SYBR green supermix, which were commercially available from Biorad (USA). Animals were purchased from GemPharmatech (China). Chlorin e6 (Ce6) was purchased from Shanghai Yuanye Bio-Technology (China). 1,2-distearoyl-sn-glycero-3-phosphoethanolamine-N-[methoxy (polyethylene glycol)-2000] (DSPE-mPEG2000), 1, 2-dioleoyl-sn-glycero-3-phosphoethanolamine (DOPE) and cholesterol were bought from A.V.T. Pharmaceutical Co., Ltd (China).

Synthesis of CD Prodrug Conjugation (RSCD): Boc/Pbf-Arg-OH (6 g, 11 mmol), H-Lys-OMe-2HCl (1.2 g, 5 mmol), DIEA (1.9 g, 15 mmol), and HBTU (5.7 g, 15 mmol) were weighed accurately and dissolved in anhydrous dimethylformamide (50 mL). The mixed solution was stirred at 30 °C for 5 h under nitrogen atmosphere, and then concentrated in vacuum. The obtained residue was re-dissolved in dichloromethane (100 mL) and washed by saturated NaHCO₃ (aq), dilute hydrochloric acid, and saturated brine solution, sequentially. The collected organic layer was dried with MgSO₄, concentrated and purified by silica gel column

chromatography (dichloromethane: methanol = 15:1 v/v) to obtain a white powder (compound 1, 56.1% yield). Compound 1 (3 g, 2.5 mmol) and NaOH (0.8 g, 20 mmol) were dissolved in methanol (10 mL) for 6 h reaction, and the solution was concentrated under reduced pressure. The obtained residue was re-dissolved in H₂O (125 mL), and the pH value of solution was adjusted to 7 by diluted hydrochloric acid. The aqueous solution was extracted with dichloromethane (250 mL). While organic phase was separated, dried with MgSO₄ and concentrated by rotary evaporator to obtain compound 2 (2.67 g, 89% yield).

To a solution of CD (0.44 g, 1 mmol), the mixture of Boc-Cystamine (0.28 g, 1.1 mmol), and HBTU (0.75 g, 2.0 mmol) in anhydrous dichloromethane (50 mL) was added with DIEA (0.26 g, 1.98 mmol). The reaction system was stirred overnight at room temperature and concentrated by a rotary evaporator. The resultant residue was re-dissolved in dichloromethane and washed by saturated NaHCO₃ (aq), dilute hydrochloric acid, and saturated brine solution, sequentially. The collected organic layer was dried with MgSO₄ and concentrated to obtain the crude product. Then the purified product was obtained by column chromatography and re-dissolved in the mixture of TFA (5 mL) and dichloromethane (2 mL) for 24 h-deprotection with stirring. The solution was then concentrated and precipitated with ether to give a white powder. (compound 3, 0.34 g, 60% yield). Compound 2 (0.7 g, 0.6 mmol), compound 3 (0.3 g, 0.5 mmol), DIEA (0.12 g, 1.1 mmol), and HBTU (0.42 g, 1.1 mmol) were dissolved in anhydrous dimethylformamide (25 mL) under nitrogen atmosphere, and stirred for 48 h at room temperature. Organic solvents were removed in vacuum. The resultant residue was re-dissolved in dichloromethane, washed as above method, dried with MgSO₄ and concentrated by a rotary evaporator. After purification by column chromatography, compound 4 was obtained. (0.47 g, 55% yield). It (Compound 4, 0.45 g) was re-dissolved in the mixed solution of TFA (5 mL) and dichloromethane (2 mL) to remove the N-tert-butoxycarbonyl group. After that, the reaction solution was concentrated and precipitated with ether to produce a white powder. (RSCD, 0.32 g, 60% yield) The structures of compounds were characterized by nuclear magnetic resonance (NMR) spectrometry as well as matrix-assisted laser desorption/ionization time of flight mass spectrometry (MALDI-TOF MS).

Fabrication and Characterization of CD Analog Based Cationic Assemblies: The preparation of CD analog-based assemblies was according to the typical injection method with some modifications. First of all, an appropriate amount of amphiphilic molecules (RSCD) was dissolved in methanol and further mixed with RLS. The methanol solution was injected into a RNase-free HBG solution (1 mL, 20 mM HEPES, pH 7.4, 5% glucose) for 1 h fast stirring. Cationic assemblies were formed spontaneously in the aqueous medium. Particle size and zeta potential of the RSCD cationic assemblies were characterized by dynamic light scattering using a Zetasizer Nano ZS (Malvern Instruments, Worcestershire, UK). Besides, the assemblies were dropped on copper grid for morphology observation by TEM (JM-1011, JEOL).

Assembly and Characterization of siRNA Complexes: RSCD/siRNA complexes were prepared by mixing siRNA and RSCD cationic assemblies gently at different N/P ratios in HBG buffer, and incubated for 30 min at room temperature before use. And then, the HA-SS-COOH was dropwise added into the pre-prepared binary complexes to form HA-RSCD/siRNA ternary complexes. Size distribution as well as zeta potential of HA-RSCD/siRNA and RSCD/siRNA complexes were assessed by a Zetasizer Nano-ZS (Malvern Instruments, U.K.) at a final siRNA concentration of 3 μg mL⁻¹. The siRNA compaction ability in complexes at various N/P ratios was evaluated by gel retardation assay, using 1% agarose gel for electrophoresis (120 V, 0.5 h). The gel was stained with GelRed, and observed by the Molecular Imager ChemiDoc XRS+ (Bio-Rad, USA).

Redox Responsiveness of the Cationic Complexes: In order to evaluate the responsiveness of RSCD and HA-RSCD complexes in reductive conditions, they (with concentration of 1 mg mL⁻¹) were incubated with GSH (10 mM) at 37 °C. The changes of particle size and zeta potential were measured by Zetasizer Nano-ZS at indicated time points.

In addition, the release profiles of siRNA from RSCD and HA-RSCD complexes were further evaluated by gel electrophoresis assay after 2 h GSH incubation (10 mM) at 37 °C.

Release of CD from HA-RSCD and RSCD Assemblies: The *in vitro* release of CD was performed in PBS with GSH and amidase in a time-course procedure. The resulting solution was gently shaken in a 37 °C a water bath at 100 rpm. At every predetermined time point, aliquots (1 mL) withdrawn from one sample were mixed with 1 mL methanol to extract the released CD. HPLC was used for the measurement of CD concentration in the solution with a 256 nm UV detector. The mobile phase was methanol and water containing 1% phosphoric acid (volume ratio 66:34) at a flow rate of 1 mL min⁻¹.

Cellular Uptake and Intracellular Tracking Study of HA-RSCD and RSCD Complexes: CLSM was employed for study of cellular uptake and intracellular tracking. HepG2 cells were seeded into a 3.5 cm confocal dish at a concentration of 1 × 10⁴ cells mL⁻¹. And then cells were replaced with fresh medium with 10% serum containing various Cy5-labeled nanocomplexes containing 0.2 μg siRNA at 37 °C. At indicated time points, the cells were washed with cold PBS to remove the nanocomplexes that were not taken. The lysosomes and nucleus were stained with Green Lyso Tracker and Hoechst 33342, respectively, which were observed by CLSM.

In Vitro HIF-1α Silencing and VEGF Downregulation Efficiency with Hypoxia Stress: HepG2 cells were seeded into 6-well plates and cultured overnight for cell adhesion with ≈70% confluence. Varying transfection formulations carrying 2 μg siHIF-1α or 2 μM CD were added into fresh culture medium containing 100 μM CoCl₂ for 24 h^[51] (mRNA extraction) or 48 h (protein extraction) treatment. The expression of HIF-1α and VEGF were determined by quantitative real-time PCR (qRT-PCR) and WB, respectively.

In Vitro Cytotoxicity: The cytotoxicity of HA-RSCD/siHIF-1α complexes was evaluated against HUVEC and HepG2 cells using CCK-8 Assay. Cells were seeded on 96 well-plates at the density of 1 × 10⁴ cells per well. After incubation for 24 h, the old medium was replaced with 100 μL of fresh growth medium containing various formulations or condition medium. Concentrations/amounts of CD and/or siRNA in each well were 2 μM for CD and 0.2 μg for siRNA. After incubation at 37 °C for 24 h, the medium was replaced with fresh one (90 μL) and 10 μL of CCK-8 (Dojindo Molecular Technologies, Japan), and the cells were incubated for 2 h at 37 °C. The absorbance was measured at 450 nm using a microplate reader (Bio-Rad, model 550, USA). The cytotoxicity test was performed in 5 replicates of each sample. The cells without any treatment were used as a control (100% cell viability), and the cell viability was expressed as a percentage of the control.

In Vitro Angiogenesis Assay: Tube formation assay was employed to assess the effect of various formulations on HUVEC vascularization. Liquefied matrigel matrix was first placed into precooled 96 well plates (50 μL well⁻¹) followed with 30 min incubation at 37 °C for solidifying. HUVEC cells transfected with different formulations were then digested and seeded onto the matrigel coated plates for tubule formation in 4 h. HUVEC cells also were treated with the supernatants of HepG2 cells (condition medium) after transfection with different formulations. Concentrations/amounts of CD and/or siRNA in each well were 2 μM for CD and 0.2 μg for siRNA. The untreated HUVEC cells were served as control group. Images of tubule formation were observed by an inverted bright field microscope (Leica) and the TL was processed by Image J software. The inhibitory rate of tubule structure formation was calculated using the following formula:

$$\text{Inhibitory rate(\%)} = \frac{(TL_{\text{control}} - TL_{\text{sample}})}{TL_{\text{control}}} \times 100\% \quad (1)$$

Migration Property of Vascular Endothelial Cells and Tumor Cells: HUVEC cells transfected with different formulations containing 2 μM CD or 0.2 μg siRNA were collected and suspended at a final concentration of 1 × 10⁷ cells L⁻¹ in fresh ECM. HUVEC cells were loaded into the top wells of Boyden chamber, and ECM with 0.1 mM Ang II was placed into the bottom wells with 4 h chemotaxis. HUVEC cells also were cultured with the supernatants of HepG2 cells (condition medium) after transfection

by different formulations. Cells retaining on upper surface of the top well membranes were swabbed to remove. Cells migrated onto the lower surface were fixed and stained with crystal violet for optical microscope observation.

Therapeutic Effects of HA-RSCD/siHIF-1 α Complexes In Vivo: Female BALB/c nude mice (5 weeks old, \approx 20 g) were purchased from Chengdu Dossy Experimental Animals CO., LTD [License numbers: SCXK (Chuan) 2020-030]. All animal experiment procedures were performed in accordance with the Guidelines for Care and Use of Laboratory Animals of West China Hospital of Sichuan University, and approved by the Biomedical Research Ethics Committee of West China Hospital of Sichuan University (No. 2018-078). Female BALB/c nude mice were inoculated with HepG2 cells by subcutaneous injection of 1×10^6 cells. Once the tumor volume reached, on average, \approx 100 mm³ (width \times length \times width/2), treatment was then performed by intratumor injection of saline, HA-RSCD/siHIF-1 α , RSCD/siHIF-1 α , RLS/siHIF-1 α plus CD at a siRNA dose of 2.5 mg kg⁻¹ and CD dose of 2 mg kg⁻¹ every other day, respectively. Mice were randomly divided into four groups with 5 mice in each group. The tumor volume as well as mice body weight were monitored throughout the study. At the end of the therapy period, mice were sacrificed and tumor mass was harvested for pathological and immunohistochemistry analysis.

Tumor Oxygenation: For tumor hypoxia study, 1 h before tumors were surgically excised from the mice with different formulations pretreatment, pimonidazole hydrochloride (60 mg kg⁻¹) (hypoxyprobe-1 plus kit, hypoxyprobe Inc), which would form stable adducts with thiol (sulfhydryl) groups in biomolecules, was injected through the caudal vein into the mice. Then, tumor sections were processed for paraffin sections and incubated with mouse anti-pimonidazole antibody following the manufacturer's instructions.

Tumor oxygenation was also evaluated by PA. The signal of oxygenated hemoglobin (HbO₂) and Hb in tumor tissue for different groups was detected by multispectral photoacoustic tomography (MSOT in Vision 128, iTheramedical, Germany). In vivo PA was carried out using Oxyhem mode with excitation wavelengths of 750 and 850 nm, respectively. The photoacoustic signal ratio between HbO₂ and total hemoglobin was used to calculate the level of oxygen saturation across the tumor area (sO₂) as follows: $[sO_2] = [HbO_2] / ([HbO_2] + [Hb])$.

Combination Therapy of HA-RSCD/siHIF-1 α Complexes and Doxorubicin: The antitumor efficacy of the HA-RSCD/siHIF-1 α complexes combined with doxorubicin was evaluated in the HepG2 subcutaneous xenograft tumor model. Once the tumor volume reached, on average, \approx 100 mm³, the mice were randomly divided into three groups with 5 mice in each group. In the first group, mice were intravenously administrated (i.v.) normal saline every other day for seven doses; The second group was intratumorally administrated (i.t.) normal saline for three doses and following doxorubicin treatment for four doses (i.v. 5 mg kg⁻¹); The last group underwent intratumor administration of HA-RSCD/siHIF-1 α complexes for three doses and doxorubicin treatment for four doses (i.v. 5 mg kg⁻¹). Tumor sizes as well as body weights were monitored throughout the treatment. Animals were sacrificed 48 h after the last treatment. Tumor tissues were fixed by 4% paraformaldehyde overnight, dehydrated by gradient alcohol, embedded by paraffin, and concomitantly cut into 5 μ m sections for H&E staining and TUNEL analysis.

Doxorubicin Intratumoral Accumulation in Combination Therapy: Doxorubicin (10 mg kg⁻¹) was intravenously administrated into the mice pre-treated with HA-RSCD/siHIF-1 α complexes or saline for three times. The biodistribution of doxorubicin was evaluated at 2 h, 6 h, 8 h, and 24 h post-injection by IVIS Lumina Series III imaging system (PerkinElmer, USA). Mice were then sacrificed after 24 h post-injection and tumor tissues as well as, major organs including heart, liver, spleen, lung, and kidney were harvested for ex vivo imaging and quantitative analysis by using the IVIS imaging system.

Preparation of Ce6 Liposome: The liposome composed of DOPE/cholesterol/DSPE-mPEG_{2k} at molar ratio of 3:1:1 was prepared by thin-film dispersion method. Briefly, 1 mg Ce6 was dissolved in methanol (2 mL) and then mixed with the 2 mL chloroform solution of lipid

mixture (40 mg) in a round flask. The mixture was subsequently evaporated to remove the organic solvent. HEPES-buffered saline was added to the formed thin film, and the mixture was sonicated for 20 min at 40 °C. The resulting suspension of Ce6 liposome was stored at 4 °C in the dark until use.

In Vivo Biodistribution of Ce6 Liposome in the Combination Therapy with HA-RSCD/siHIF-1 α : The biodistribution of Ce6 liposome in vivo was detected by IVIS Lumina Series III imaging system (PerkinElmer, USA). Ce6 liposome (5 mg kg⁻¹) was intravenously injected into the mice pre-treated with HA-RSCD/siHIF-1 α complexes or saline for three times. At the predetermined time point, fluorescence images were taken at an excitation of 640 nm and emission of 710 nm.

Combination Therapy of HA-RSCD/siHIF-1 α Complexes and Ce6 Induced PDT: Chlorin e6 (Ce6) was chosen as a photosensitizer to investigate whether the reconstruction of tumor suppressing microenvironment by HA-RSCD/siHIF-1 α could enhance the therapeutic effects of liposomal Ce6-mediated PDT. The hepatic tumor xenograft model was constructed as described above. When tumor grew to around 100 mm³, the mice were randomly divided into two groups (10 mice per group) for the relaxation therapy: 1) Saline; 2) HA-RSCD/siHIF-1 α with three dosages every other day. After that, mice were divided into four groups: 1) Saline; 2) PDT; 3) HA-RSCD/siHIF-1 α ; 4) HA-RSCD/siHIF-1 α + Ce6 liposomes-mediated PDT. Ce6 was intravenously administrated at dosage of 5 mg kg⁻¹ after 24 h following the last relaxation therapy. And PDT was next performed with one day interval with 660 nm laser irradiation for 30 min at a power density of 100 mW cm⁻². During the treatment, the body weight of each group was weighed and the tumor volume was measured every other day for 14 days. Animals were sacrificed 48 h after the last treatment. Tumor tissues were fixed by 4% paraformaldehyde overnight, dehydrated by gradient alcohol, embedded by paraffin, and concomitantly cut into 5 μ m sections for H&E and TUNEL analysis.

Statistics Analysis: Data are presented as means with standard deviations (SD) with at least five independent samples, and each measurement was performed in triplicate. Data sets were compared using two-tailed, unpaired t tests under assumption of equal variance. A *p* value of < 0.05 was considered to be statistically significant.

Supporting Information

Supporting Information is available from the Wiley Online Library or from the author.

Acknowledgements

X.C. and R.J. contributed equally to this work. This study was supported by National Key Research and Development Program of China (2017YFC1104601), National Natural Science Foundation of China (NSFC, No. 81873921, 51933011, and 51903174), Sino-German cooperation group project (GZ1512), Sichuan Science and Technology Program (2019JDQ0027 and 2019JDTD0008), and Chengdu International Cooperation Program (2020-GH02-00007-HZ). The authors also thank the Analytical & Testing Center of Sichuan University for sample analysis.

Conflict of Interest

The authors declare no conflict of interest.

Data Availability Statement

Research data are not shared.

Keywords

candesartan conjugation, chemotherapy, photodynamic therapy, siHIF-1 α delivery, tumor micro-environment reconstruction

Received: January 30, 2021
Revised: February 17, 2021
Published online: May 25, 2021

- [1] A. Patel, S. Sant, *Biotechnol. Adv.* **2016**, *34*, 803.
[2] E. L. Lagory, A. J. Giaccia, *Nat. Cell Biol.* **2016**, *18*, 356..
[3] S. M. Weis, D. A. Cheresch, *Nat. Med.* **2011**, *17*, 1359.
[4] S. Kizaka-Kondoh, S. Tanaka, H. Harada, M. Hiraoka, *Adv. Drug Delivery Rev.* **2009**, *61*, 623.
[5] J. D. Martin, G. Seano, R. K. Jain, *Annu. Rev. Physiol.* **2019**, *81*, 505.
[6] P. Ofek, G. Tiram, R. Satchi-Fainaro, *Adv. Drug Delivery Rev.* **2017**, *119*, 3.
[7] R. , Chen, L. , Huang, K. , Hu, *Acta Pharm. Sin. B* **2020**, *10*, 2140.
[8] G. C. Jayson, R. Kerbel, L. M. Ellis, A. L. Harris, *Lancet* **2016**, *388*, 518.
[9] T. Bohn, S. Rapp, N. Luther, M. Klein, T.-J. Bruehl, N. Kojima, P. Aranda Lopez, J. Hahlbrock, S. Muth, S. Endo, S. Pektor, A. Brand, K. Renner, V. Popp, K. Gerlach, D. Vogel, C. Lueckel, D. Arnold-Schild, J. Pouyssegur, M. Kreutz, M. Huber, J. Koenig, B. Weigmann, H.-C. Probst, E. von Stebut, C. Becker, H. Schild, E. Schmitt, T. Bopp, *Nat. Immunol.* **2018**, *19*, 1319.
[10] R. K. Jain, *Cancer Cell* **2014**, *26*, 605.
[11] R. K. Jain, *Science* **2005**, *307*, 58.
[12] Q. Chen, L. Xu, J. Chen, Z. Yang, C. Liang, Y. Yang, Z. Liu, *Biomaterials* **2017**, *148*, 69.
[13] X. Luan, Y.-Y. Guan, J. F. Lovell, M. Zhao, Q. Lu, Y.-R. Liu, H.-J. Liu, Y.-G. Gao, X. Dong, S.-C. Yang, L. Zheng, P. Sun, C. Fang, H.-Z. Chen, *Biomaterials* **2016**, *95*, 60.
[14] B. Wang, Y. Ding, X. Zhao, X. Han, N. Yang, Y. Zhang, Y. Zhao, X. Zhao, M. Taleb, Q. R. Miao, G. Nie, *Biomaterials* **2018**, *175*, 110.
[15] S. Du, H. Xiong, C. Xu, Y. Lu, J. Yao, *Biomater. Sci.* **2019**, *7*, 1147.
[16] X. Ding, Y. Su, C. Wang, F. Zhang, K. Chen, Y. Wang, M. Li, W. Wang, *ACS Appl. Mater. Interfaces* **2017**, *9*, 23353.
[17] Y. Su, Y. Hu, Y. Wang, X. Xu, Y. Yuan, Y. Li, Z. Wang, K. Chen, F. Zhang, X. Ding, M. Li, J. Zhou, Y. Liu, W. Wang, *Biomaterials* **2017**, *139*, 75.
[18] A. Ahmed, A. A. Ahmad, G. Anna, G. Fei, S. C. Fagan, P. R. Somanath, *J. Pharmacol. Exp. Ther.* **2014**, *350*, 635.
[19] V. P. Chauhan, J. D. Martin, H. Liu, D. A. Lacorre, S. R. Jain, S. V. Kozin, T. Stylianopoulos, A. S. Mousa, X. Han, P. Adstamongkonkul, *Nat. Commun.* **2013**, *4*, 2516.
[20] V. P. Chauhan, I. X. Chen, R. Tong, M. R. Ng, J. D. Martin, K. Naxerova, M. W. Wu, P. Huang, Y. Boucher, D. S. Kohane, R. Langer, R. K. Jain, *Proc. Natl. Acad. Sci. U. S. A.* **2019**, *116*, 10674.
[21] J. J. Shi, P. W. Kantoff, R. Wooster, O. C. Farokhzad, *Nat. Rev. Cancer* **2017**, *17*, 20.
[22] G. N. Masoud, W. Li, *Acta Pharm. Sin. B* **2015**, *5*, 378.
[23] V. Petrova, M. Annicchiarico-Petruzzelli, G. Melino, I. Amelio, *Oncogenesis* **2018**, *7*, 10.
[24] V. M. Shah, B. C. Sheppard, R. C. Sears, A. W. G. Alani, *Cancer Lett.* **2020**, *492*, 63.
[25] A. Sahu, I. Kwon, G. Tae, *Biomaterials* **2020**, *228*, 119578.
[26] V. P. Chauhan, R. K. Jain, *Nat. Mater.* **2013**, *12*, 958.
[27] Z. Zhou, J. Song, L. Nie, X. Chen, *Chem. Soc. Rev.* **2016**, *45*, 6597.
[28] X. Chen, J. Yang, H. Liang, Q. Jiang, B. Ke, Y. Nie, *J. Mater. Chem. B* **2017**, *5*, 1482.
[29] H. Liang, X. Chen, R. Jin, B. Ke, M. Barz, H. Ai, Y. Nie, *Small* **2020**, *16*, 1906538.
[30] O. Schäfer, M. Barz, *Chem. - Eur. J.* **2018**, *24*, 12131.
[31] Q. Bi, X. Song, A. Hu, T. Luo, Y. Nie, *Chin. Chem. Lett.* **2020**, *31*, 3041.
[32] Y. Y. Cheng, L. B. Zhao, Y. W. Li, T. W. Xu, *Chem. Soc. Rev.* **2011**, *40*, 2673.
[33] Q. Jiang, X. Chen, H. Liang, Y. Nie, R. Jin, M. Barz, D. Yue, Z. Gu, *Nanoscale Adv.* **2019**, *1*, 498.
[34] Q. Jiang, D. Yue, Y. Nie, X. Xu, Y. He, S. Zhang, E. Wagner, Z. Gu, *Mol. Pharmaceutics* **2016**, *13*, 1809.
[35] X. Xu, Q. Jiang, X. Zhang, Y. Nie, Z. Zhang, Y. Li, G. Cheng, Z. Gu, *J. Mater. Chem. B* **2015**, *3*, 7006.
[36] H. Liang, Q. Bi, A. Hu, X. Chen, R. Jin, X. Song, B. Ke, M. Barz, Y. Nie, *Chem. Commun.* **2020**, *56*, 6949.
[37] X. Bao, W. Wang, C. Wang, Y. Wang, J. Zhou, Y. Ding, X. Wang, Y. Jin, *Biomaterials* **2014**, *35*, 8450.
[38] Q. Song, X. Wang, Y. Wang, Y. Liang, Q. Zhang, *Mol. Pharmaceutics* **2015**, *13*, 190.
[39] S. Ganesh, A. K. Iyer, D. V. Morrissey, M. M. Amiji, *Biomaterials* **2013**, *34*, 3489.
[40] S. Wang, Y. Tian, W. Tian, J. Sun, S. Zhao, Y. Liu, C. Wang, Y. Tang, X. Ma, Z. Teng, *ACS Nano* **2016**, *10*, 8578.
[41] Y. Hu, J. Liu, H. Huang, *J. Cell. Biochem.* **2013**, *114*, 498.
[42] Y. He, G. Cheng, L. Xie, Y. Nie, B. He, Z. Gu, *Biomaterials* **2013**, *34*, 1235.
[43] F. Dai, R. K. Jain, *J. Cell. Biochem.* **2007**, *101*, 937.
[44] M. D. Palma, D. Bizziato, T. V. Petrova, *Nat. Rev. Cancer* **2017**, *17*, 457.
[45] Z. K. Otrrock, H. A. Hatoum, A. H. Awada, R. S. Ishak, A. I. Shamseddine, *Crit. Rev. Oncol. Hematol.* **2009**, *70*, 93.
[46] G. Jiang, K. Park, J. Kim, K. S. Kim, S. K. Hahn, *Mol. Pharmaceutics* **2009**, *6*, 727.
[47] R. Du, K. V. Lu, C. Petritsch, P. Liu, R. Ganss, E. Passequé, H. Song, S. VandenBerg, R. S. Johnson, Z. Werb, G. Bergers, *Cancer Cell* **2008**, *13*, 206.
[48] F. Maione, F. Molla, C. Meda, R. Latini, L. Zentilin, M. Giacca, G. Seano, G. Serini, F. Bussolino, E. Giraudo, *J. Clin. Invest.* **2009**, *119*, 3356.
[49] J. Yang, W. Li, L. Luo, M. Jiang, C. Zhu, B. Qin, H. Yin, X. Yuan, X. Yin, J. Zhang, Z. Luo, Y. Du, J. You, *Biomaterials* **2018**, *182*, 145.
[50] Y. He, Y. Nie, L. Xie, H. Song, Z. Gu, *Biomaterials* **2014**, *35*, 1657.
[51] X. Q. Liu, M. H. Xiong, X. T. Shu, R. Z. Tang, J. Wang, *Mol. Pharmaceutics* **2012**, *9*, 2863.